Measurement of branching fractions of $\Lambda_c^+ \to \eta\Lambda\pi^+$, $\eta\Sigma^0\pi^+$, $\Lambda(1670)\pi^+$, and $\eta\Sigma(1385)^+$

J. Y. Lee,[77] K. Tanida,[35] Y. Kato,[57] S. K. Kim,[77] S. B. Yang,[42,*] I. Adachi,[19,15] J. K. Ahn,[42] H. Aihara,[89] S. Al Said,[83,40] D. M. Asner,[3] T. Aushev,[21] R. Ayad,[83] V. Babu,[8] S. Bahinipati,[25] P. Behera,[28] C. Beleño,[14] J. Bennett,[54] M. Bessner,[18] B. Bhuyan,[26] T. Bilka,[5] J. Biswal,[36] G. Bonvicini,[93] A. Bozek,[63] M. Bračko,[51,36] T. E. Browder,[18] M. Campajola,[33,58] L. Cao,[2] D. Červenkov,[5] M.-C. Chang,[11] P. Chang,[62] V. Chekelian,[52] A. Chen,[60] B. G. Cheon,[17] K. Chilikin,[46] K. Cho,[41] S.-K. Choi,[16] Y. Choi,[81] S. Choudhury,[27] D. Cinabro,[93] S. Cunliffe,[8] G. De Nardo,[33,58] F. Di Capua,[33,58] Z. Doležal,[5] T. V. Dong,[12] S. Eidelman,[4,67,46] D. Epifanov,[4,67] T. Ferber,[8] B. G. Fulsom,[69] R. Garg,[70] V. Gaur,[92] A. Garmash,[4,67] A. Giri,[27] P. Goldenzweig,[37] B. Golob,[48,36] C. Hadjivasiliou,[69] O. Hartbrich,[18] K. Hayasaka,[65] H. Hayashii,[59] M. T. Hedges,[18] M. Hernandez Villanueva,[54] C.-L. Hsu,[82] K. Inami,[57] A. Ishikawa,[19,15] R. Itoh,[19,15] M. Iwasaki,[68] W. W. Jacobs,[29] E.-J. Jang,[16] S. Jia,[12] Y. Jin,[89] C. W. Joo,[38] K. K. Joo,[6] K. H. Kang,[44] G. Karyan,[8] H. Kichimi,[19] C. Kiesling,[52] B. H. Kim,[77] D. Y. Kim,[80] K.-H. Kim,[95] K. T. Kim,[42] S. H. Kim,[77] Y. J. Kim,[42] Y.-K. Kim,[95] K. Kinoshita,[7] P. Kodyš,[5] S. Korpar,[51,36] D. Kotchetkov,[18] P. Križan,[48,36] R. Kroeger,[54] P. Krokovny,[4,67] T. Kuhr,[49] R. Kulasiri,[39] K. Kumara,[93] A. Kuzmin,[4,67] Y.-J. Kwon,[95] S. C. Lee,[44] C. H. Li,[47] L. K. Li,[7] Y. B. Li,[71] L. Li Gioi,[52] J. Libby,[28] K. Lieret,[49] Z. Liptak,[18,†] D. Liventsev,[93,19] T. Luo,[12] C. MacQueen,[53] M. Masuda,[88,73] T. Matsuda,[55] D. Matvienko,[4,67,46] M. Merola,[33,58] K. Miyabayashi,[59] R. Mizuk,[46,21] G. B. Mohanty,[84] T. J. Moon,[77] T. Mori,[57] R. Mussa,[34] T. Nakano,[73] M. Nakao,[19,15] A. Natochii,[18] M. Nayak,[86] M. Niiyama,[43] N. K. Nisar,[3] S. Nishida,[19,15] K. Ogawa,[65] S. Ogawa,[87] S. L. Olsen,[16] H. Ono,[64,65] Y. Onuki,[89] P. Oskin,[46] P. Pakhlov,[46,56] G. Pakhlova,[21,46] S. Pardi,[33] S.-H. Park,[95] S. Patra,[24] S. Paul,[85,52] T. K. Pedlar,[50] R. Pestotnik,[36] L. E. Piilonen,[92] T. Podobnik,[48,36] V. Popov,[21] E. Prencipe,[22] M. T. Prim,[37] A. Rostomyan,[8] N. Rout,[28] G. Russo,[58] D. Sahoo,[84] Y. Sakai,[19,15] S. Sandilya,[7,27] A. Sangal,[7] L. Santelj,[48,36] V. Savinov,[72] G. Schnell,[1,23] J. Schueler,[18] C. Schwanda,[31] A. J. Schwartz,[7] R. Seidl,[75] Y. Seino,[65] K. Senyo,[94] M. E. Sevior,[53] M. Shapkin,[32] V. Shebalin,[18] J.-G. Shiu,[62] B. Shwartz,[4,67] A. Sokolov,[32] E. Solovieva,[46] S. Stanič,[66] M. Starič,[36] Z. S. Stottler,[92] M. Sumihama,[13] T. Sumiyoshi,[91] W. Sutcliffe,[2] M. Takizawa,[78,20,74] U. Tamponi,[34] F. Tenchini,[8] M. Uchida,[90] T. Uglov,[46,21] S. Uno,[19,15] Y. Usov,[4,67] S. E. Vahsen,[18] R. Van Tonder,[2] G. Varner,[18] A. Vinokurova,[4,67] V. Vorobyev,[4,67,46] A. Vossen,[9] C. H. Wang,[61] E. Wang,[72] M.-Z. Wang,[62] P. Wang,[30] M. Watanabe,[65] S. Watanuki,[45] S. Wehle,[8] J. Wiechczynski,[63] X. Xu,[79] B. D. Yabsley,[82] W. Yan,[76] H. Ye,[8] J. Yelton,[10] J. H. Yin,[42] C. Z. Yuan,[30] Y. Yusa,[65] Z. P. Zhang,[76] V. Zhilich,[4,67] V. Zhukova,[46] and V. Zhulanov[4,67]

(Belle Collaboration)

[1]*University of the Basque Country UPV/EHU, 48080 Bilbao*
[2]*University of Bonn, 53115 Bonn*
[3]*Brookhaven National Laboratory, Upton, New York 11973*
[4]*Budker Institute of Nuclear Physics SB RAS, Novosibirsk 630090*
[5]*Faculty of Mathematics and Physics, Charles University, 121 16 Prague*
[6]*Chonnam National University, Gwangju 61186*
[7]*University of Cincinnati, Cincinnati, Ohio 45221*
[8]*Deutsches Elektronen–Synchrotron, 22607 Hamburg*
[9]*Duke University, Durham, North Carolina 27708*
[10]*University of Florida, Gainesville, Florida 32611*
[11]*Department of Physics, Fu Jen Catholic University, Taipei 24205*
[12]*Key Laboratory of Nuclear Physics and Ion-beam Application (MOE) and Institute of Modern Physics, Fudan University, Shanghai 200443*
[13]*Gifu University, Gifu 501-1193*
[14]*II. Physikalisches Institut, Georg-August-Universität Göttingen, 37073 Göttingen*
[15]*SOKENDAI (The Graduate University for Advanced Studies), Hayama 240-0193*
[16]*Gyeongsang National University, Jinju 52828*
[17]*Department of Physics and Institute of Natural Sciences, Hanyang University, Seoul 04763*
[18]*University of Hawaii, Honolulu, Hawaii 96822*
[19]*High Energy Accelerator Research Organization (KEK), Tsukuba 305-0801*
[20]*J-PARC Branch, KEK Theory Center, High Energy Accelerator Research Organization (KEK), Tsukuba 305-0801*
[21]*Higher School of Economics (HSE), Moscow 101000*
[22]*Forschungszentrum Jülich, 52425 Jülich*

[23]*IKERBASQUE, Basque Foundation for Science, 48013 Bilbao*
[24]*Indian Institute of Science Education and Research Mohali, SAS Nagar, 140306*
[25]*Indian Institute of Technology Bhubaneswar, Satya Nagar 751007*
[26]*Indian Institute of Technology Guwahati, Assam 781039*
[27]*Indian Institute of Technology Hyderabad, Telangana 502285*
[28]*Indian Institute of Technology Madras, Chennai 600036*
[29]*Indiana University, Bloomington, Indiana 47408*
[30]*Institute of High Energy Physics, Chinese Academy of Sciences, Beijing 100049*
[31]*Institute of High Energy Physics, Vienna 1050*
[32]*Institute for High Energy Physics, Protvino 142281*
[33]*INFN—Sezione di Napoli, 80126 Napoli*
[34]*INFN—Sezione di Torino, 10125 Torino*
[35]*Advanced Science Research Center, Japan Atomic Energy Agency, Naka 319-1195*
[36]*J. Stefan Institute, 1000 Ljubljana*
[37]*Institut für Experimentelle Teilchenphysik, Karlsruher Institut für Technologie, 76131 Karlsruhe*
[38]*Kavli Institute for the Physics and Mathematics of the Universe (WPI), University of Tokyo, Kashiwa 277-8583*
[39]*Kennesaw State University, Kennesaw, Georgia 30144*
[40]*Department of Physics, Faculty of Science, King Abdulaziz University, Jeddah 21589*
[41]*Korea Institute of Science and Technology Information, Daejeon 34141*
[42]*Korea University, Seoul 02841*
[43]*Kyoto Sangyo University, Kyoto 603-8555*
[44]*Kyungpook National University, Daegu 41566*
[45]*Université Paris-Saclay, CNRS/IN2P3, IJCLab, 91405 Orsay*
[46]*P.N. Lebedev Physical Institute of the Russian Academy of Sciences, Moscow 119991*
[47]*Liaoning Normal University, Dalian 116029*
[48]*Faculty of Mathematics and Physics, University of Ljubljana, 1000 Ljubljana*
[49]*Ludwig Maximilians University, 80539 Munich*
[50]*Luther College, Decorah, Iowa 52101*
[51]*University of Maribor, 2000 Maribor*
[52]*Max-Planck-Institut für Physik, 80805 München*
[53]*School of Physics, University of Melbourne, Victoria 3010*
[54]*University of Mississippi, University, Mississippi 38677*
[55]*University of Miyazaki, Miyazaki 889-2192*
[56]*Moscow Physical Engineering Institute, Moscow 115409*
[57]*Graduate School of Science, Nagoya University, Nagoya 464-8602*
[58]*Università di Napoli Federico II, 80126 Napoli*
[59]*Nara Women's University, Nara 630-8506*
[60]*National Central University, Chung-li 32054*
[61]*National United University, Miao Li 36003*
[62]*Department of Physics, National Taiwan University, Taipei 10617*
[63]*H. Niewodniczanski Institute of Nuclear Physics, Krakow 31-342*
[64]*Nippon Dental University, Niigata 951-8580*
[65]*Niigata University, Niigata 950-2181*
[66]*University of Nova Gorica, 5000 Nova Gorica*
[67]*Novosibirsk State University, Novosibirsk 630090*
[68]*Osaka City University, Osaka 558-8585*
[69]*Pacific Northwest National Laboratory, Richland, Washington 99352*
[70]*Panjab University, Chandigarh 160014*
[71]*Peking University, Beijing 100871*
[72]*University of Pittsburgh, Pittsburgh, Pennsylvania 15260*
[73]*Research Center for Nuclear Physics, Osaka University, Osaka 567-0047*
[74]*Meson Science Laboratory, Cluster for Pioneering Research, RIKEN, Saitama 351-0198*
[75]*RIKEN BNL Research Center, Upton, New York 11973*
[76]*Department of Modern Physics and State Key Laboratory of Particle Detection and Electronics, University of Science and Technology of China, Hefei 230026*
[77]*Seoul National University, Seoul 08826*
[78]*Showa Pharmaceutical University, Tokyo 194-8543*
[79]*Soochow University, Suzhou 215006*
[80]*Soongsil University, Seoul 06978*

[81]Sungkyunkwan University, Suwon 16419
[82]School of Physics, University of Sydney, New South Wales 2006
[83]Department of Physics, Faculty of Science, University of Tabuk, Tabuk 71451
[84]Tata Institute of Fundamental Research, Mumbai 400005
[85]Department of Physics, Technische Universität München, 85748 Garching
[86]School of Physics and Astronomy, Tel Aviv University, Tel Aviv 69978
[87]Toho University, Funabashi 274-8510
[88]Earthquake Research Institute, University of Tokyo, Tokyo 113-0032
[89]Department of Physics, University of Tokyo, Tokyo 113-0033
[90]Tokyo Institute of Technology, Tokyo 152-8550
[91]Tokyo Metropolitan University, Tokyo 192-0397
[92]Virginia Polytechnic Institute and State University, Blacksburg, Virginia 24061
[93]Wayne State University, Detroit, Michigan 48202
[94]Yamagata University, Yamagata 990-8560
[95]Yonsei University, Seoul 03722

(Received 26 August 2020; accepted 28 January 2021; published 15 March 2021)

We report branching fraction measurements of four decay modes of the Λ_c^+ baryon, each of which includes an η meson and a Λ baryon in the final state, and all of which are measured relative to the $\Lambda_c^+ \to pK^-\pi^+$ decay mode. The results are based on a 980 fb^{-1} data sample collected by the Belle detector at the KEKB asymmetric-energy e^+e^- collider. Two decays, $\Lambda_c^+ \to \eta\Sigma^0\pi^+$ and $\Lambda(1670)\pi^+$, are observed for the first time, while the measurements of the other decay modes, $\Lambda_c^+ \to \eta\Lambda\pi^+$ and $\eta\Sigma(1385)^+$, are more precise than those made previously. We obtain relative branching fractions of $\mathcal{B}(\Lambda_c^+ \to \eta\Lambda\pi^+)/\mathcal{B}(\Lambda_c^+ \to pK^-\pi^+) = 0.293 \pm 0.003 \pm 0.014$, $\mathcal{B}(\Lambda_c^+ \to \eta\Sigma^0\pi^+)/\mathcal{B}(\Lambda_c^+ \to pK^-\pi^+) = 0.120 \pm 0.006 \pm 0.010$, $\mathcal{B}(\Lambda_c^+ \to \Lambda(1670)\pi^+) \times \mathcal{B}(\Lambda(1670) \to \eta\Lambda)/\mathcal{B}(\Lambda_c^+ \to pK^-\pi^+) = (5.54 \pm 0.29 \pm 0.73) \times 10^{-2}$, and $\mathcal{B}(\Lambda_c^+ \to \eta\Sigma(1385)^+)/\mathcal{B}(\Lambda_c^+ \to pK^-\pi^+) = 0.192 \pm 0.006 \pm 0.016$. The mass and width of the $\Lambda(1670)$ are also precisely determined to be $1674.3 \pm 0.8 \pm 4.9$ MeV/c^2 and $36.1 \pm 2.4 \pm 4.8$ MeV, respectively, where the uncertainties are statistical and systematic, respectively.

DOI: 10.1103/PhysRevD.103.052005

I. INTRODUCTION

The branching fractions of weakly decaying charmed baryons provide a way to study both strong and weak interactions. Although there are theoretical models that estimate the branching fractions, for example constituent quark models and heavy quark effective theories (HQET) [1,2], the lack of experimental measurements of branching fractions of charmed baryons makes it difficult to test the models. Therefore, branching fraction measurements of new decay modes of the Λ_c^+ or known decay modes with higher precision are crucial. Model-independent measurements of the branching fraction of $\Lambda_c^+ \to pK^-\pi^+$ by Belle [3] and BESIII [4] now enable branching ratios measured relative to the $\Lambda_c^+ \to pK^-\pi^+$ mode to be converted to absolute branching fraction measurements with high precision [5]. The $\Lambda_c^+ \to \eta\Lambda\pi^+$ decay mode is especially interesting since it has been suggested [6] that it is an ideal decay mode to study the $\Lambda(1670)$ and $a_0(980)$ because the isospin of any combination of two particles in the final state is unambiguous.

Two different models have been proposed to explain the structure of the $\Lambda(1670)$. One is based on a quark model and assigns it to be the SU(3) octet partner of the $N(1535)$ [7]. The other describes the $\Lambda(1670)$ as a $K\Xi$ bound state using a meson-baryon model that has also been used to describe the $\Lambda(1405)$ as a $\bar{K}N$ bound state [8]. There have been few experimental efforts to confirm the structure of the $\Lambda(1670)$; the interpretation of partial-wave analyses of $\bar{K}N$ scattering data depends on theoretical models [9,10]. Here we investigate the production and decays of the $\Lambda(1670)$ in the resonant substructure of the $\Lambda_c^+ \to \eta\Lambda\pi^+$ decay, in order to elucidate the nature of this particle.

We present measurements of branching fractions for the four decay modes, $\Lambda_c^+ \to \eta\Lambda\pi^+$, $\Lambda_c^+ \to \eta\Sigma^0\pi^+$, $\Lambda_c^+ \to \Lambda(1670)\pi^+$, and $\Lambda_c^+ \to \eta\Sigma(1385)^+$, all measured relative to the $\Lambda_c^+ \to pK^-\pi^+$ decay mode. The branching fraction of the $\Lambda_c^+ \to \Lambda(1670)\pi^+$ decay mode is given as

*Corresponding author.
sbyang@korea.ac.kr
†Present address: Hiroshima University, Higashi-Hiroshima, Hiroshima 739-8530, Japan.

the product of branching fractions of $\Lambda_c^+ \to \Lambda(1670)\pi^+$ and $\Lambda(1670) \to \eta\Lambda$ decays, $\mathcal{B}(\Lambda_c^+ \to \Lambda(1670)\pi^+) \times \mathcal{B}(\Lambda(1670) \to \eta\Lambda)$, because $\mathcal{B}(\Lambda(1670) \to \eta\Lambda)$ is not well-determined. The $\Lambda_c^+ \to \Lambda(1670)\pi^+$ and $\Lambda_c^+ \to \eta\Sigma(1385)^+$ decay modes are studied as resonant structures in the $\Lambda_c^+ \to \eta\Lambda\pi^+$ decay, while the $\Lambda_c^+ \to \eta\Sigma^0\pi^+$ decay is observed indirectly as a feed-down to the invariant mass of $\eta\Lambda\pi^+$, $M(\eta\Lambda\pi^+)$, spectrum. While $\mathcal{B}(\Lambda_c^+ \to \eta\Lambda\pi^+)$ and $\mathcal{B}(\Lambda_c^+ \to \eta\Sigma(1385)^+)$ have previously been measured by CLEO [11] and by BESIII [12], we report the first observation of the $\Lambda_c^+ \to \eta\Sigma^0\pi^+$ and $\Lambda_c^+ \to \Lambda(1670)\pi^+$ decay modes and their branching fractions. We also make precise measurements of the masses and widths of the $\Lambda(1670)$ and $\Sigma(1385)^+$.

II. DATA SAMPLE AND MONTE CARLO SIMULATION

This measurement is based on data recorded at or near the $\Upsilon(1S)$, $\Upsilon(2S)$, $\Upsilon(3S)$, $\Upsilon(4S)$, and $\Upsilon(5S)$ resonances by the Belle detector at the KEKB asymmetric-energy e^+e^- collider [13]. The total data sample corresponds to an integrated luminosity of 980 fb^{-1}. The Belle detector is a large-solid-angle magnetic spectrometer that consists of a silicon vertex detector (SVD), a central drift chamber (CDC), an array of aerogel threshold Cherenkov counters (ACC), a barrel-like arrangement of time-of-flight scintillation counters (TOF), and an electromagnetic calorimeter comprising CsI(Tl) crystals (ECL) located inside a superconducting solenoid coil that provides a 1.5 T magnetic field. An iron flux-return located outside of the coil is instrumented to detect K_L^0 mesons and to identify muons. The detector is described in detail elsewhere [14]. Two inner detector configurations were used. A 2.0-cm radius beampipe and a three-layer silicon vertex detector were used for the first sample of 156 fb^{-1}, while a 1.5-cm radius beampipe, a four-layer silicon detector and a small-cell inner drift chamber were used to record the remaining 824 fb^{-1}.

Monte Carlo (MC) simulation events are generated with PYTHIA [15] and EvtGen [16] and propagated by GEANT3 [17]. The effect of final-state radiation is taken into account in the simulation using the PHOTOS [18] package. A generic MC simulation sample, having the same integrated luminosity as real data, is used to optimize selection criteria for $\Lambda_c^+ \to \eta\Lambda\pi^+$ signal events. We also generate several signal MC simulation samples of specific Λ_c^+ decays in order to study particle reconstruction efficiencies and the detector performance; the signal MC events follow a uniform distribution in phase space.

III. EVENT SELECTION

We reconstruct Λ_c^+ candidates via $\Lambda_c^+ \to \eta\Lambda\pi^+$ decays with the η and Λ in $\eta \to \gamma\gamma$ and $\Lambda \to p\pi^-$ decays. Starting from selection criteria typically used in other charmed-hadron analyses at Belle [19,20], our final criteria are determined by a figure-of-merit (FoM) study based on the generic MC sample. We optimize the FoM, defined as $n_{\rm sig}/\sqrt{n_{\rm sig}+n_{\rm bkg}}$, where $n_{\rm sig}$ is the number of reconstructed Λ_c^+ signal events while $n_{\rm bkg}$ is the number of background events. The yields $n_{\rm sig}$ and $n_{\rm bkg}$ are counted in the $M(\eta\Lambda\pi^+)$ range from 2.2755 GeV/c^2 to 2.2959 GeV/c^2.

The η meson candidates are reconstructed from photon pairs with $M(\gamma\gamma)$ in the range 0.50–0.58 GeV/c^2 with an efficiency of 79%. A mass-constrained fit is performed to improve the momentum resolution of η candidates, and the fitted momentum and energy are used for the subsequent steps of analysis. In addition, we require η candidates to have momenta greater than 0.4 GeV/c and an energy asymmetry, defined as $|(E(\gamma_1)-E(\gamma_2))/(E(\gamma_1)+E(\gamma_2))|$, less than 0.8. For the selection of photons, the energy deposited in the ECL is required to be greater than 50 MeV for the barrel region and greater than 100 MeV for the endcap region [14]. In order to reject neutral hadrons, the ratio between energy deposited in the 3×3 array of crystals centered on the crystal with the highest energy, to that deposited in the corresponding 5×5 array of crystals, is required to be greater than 0.85. To reduce the background in the η signal region due to photons from π^0 decays, the photons used to reconstruct the η candidates are not allowed to be a part of a reconstructed π^0 with mass between 0.12 GeV/c^2 and 0.15 GeV/c^2.

Charged π^+ candidates are selected using requirements on a distance-of-closest-approach (DOCA) to the interaction point (IP) of less than 2.0 cm in the beam direction (z) and less than 0.2 cm in the transverse (r) direction. Measurements from the CDC, TOF, and ACC are combined to form particle identification (PID) likelihoods $\mathcal{L}(h)$ ($h = p^\pm$, $K^\pm$, or $\pi^\pm$), and the $\mathcal{R}(h:h')$, defined as $\mathcal{L}(h)/[\mathcal{L}(h)+\mathcal{L}(h')]$, is the ratio of likelihoods for h and h'. For the selection of π^+, $\mathcal{R}(\pi:K) > 0.2$ and $\mathcal{R}(\pi:p) > 0.4$ are required. Furthermore, the electron likelihood ratio $\mathcal{R}(e)$, defined as $\mathcal{L}(e)/[\mathcal{L}(e)+\mathcal{L}(X)]$, where $\mathcal{L}(e)$ and $\mathcal{L}(X)$ are likelihood functions for electron and nonelectron, respectively, derived from ACC, CDC, and ECL measurements [21], is required to be less than 0.7.

We reconstruct Λ candidates via $\Lambda \to p\pi^-$ decays in the mass range, $1.108\ \text{GeV}/c^2 < M(p\pi^-) < 1.124\ \text{GeV}/c^2$, and selected using Λ-momentum-dependent criteria based on four parameters: the distance between two daughter tracks along the z direction at their closest approach; the minimum distance between daughter tracks and the IP in the transverse plane; the angular difference between the Λ flight direction and the direction between the IP and the Λ decay vertex in the transverse plane; and the flight length of Λ in the transverse plane. We require $\mathcal{R}(p:\pi) > 0.6$ for the proton from the Λ decay.

Finally, η, Λ, and π^+ candidates are combined to form a Λ_c^+ with its daughter tracks fitted to a common vertex.

The χ^2 value from the vertex fit is required to be less than 40, with an efficiency of 87%. To reduce combinatorial background, especially from B meson decays, the scaled momentum $x_p = p^*/p_{\max}$ is required to be greater than 0.51; here, p^* is the momentum of Λ_c^+ in the center-of-mass frame and $p_{\max}$ is the maximum possible momentum.

Since the branching fractions are determined relative to $\mathcal{B}(\Lambda_c^+ \to pK^-\pi^+)$, Λ_c^+ candidates from $\Lambda_c^+ \to pK^-\pi^+$ decays are also reconstructed using the same selection criteria in Ref. [19] except for the scaled momentum requirement of the Λ_c^+, which is chosen to be the same as that used for the $\Lambda_c^+ \to \eta\Lambda\pi^+$ channel. All charged tracks in the $\Lambda_c^+ \to pK^-\pi^+$ decay are required to have their DOCA less than 2.0 cm and 0.1 cm in the z and r directions, respectively, and at least one SVD hit in both the z and r directions. The PID requirements are $\mathcal{R}(p:K) > 0.9$ and $\mathcal{R}(p:\pi) > 0.9$ for p, $\mathcal{R}(K:p) > 0.4$ and $\mathcal{R}(K:\pi) > 0.9$ for K, and $\mathcal{R}(\pi:p) > 0.4$ and $\mathcal{R}(\pi:K) > 0.4$ for π. In addition, $\mathcal{R}(e) < 0.9$ is required for all tracks. The charged tracks from the Λ_c^+ decay are fitted to a common vertex and the χ^2 value from the vertex fit must be less than 40.

IV. BRANCHING FRACTIONS OF $\Lambda_c^+ \to \eta\Lambda\pi^+$ AND $\eta\Sigma^0\pi^+$ MODES

The branching fractions for the $\Lambda_c^+ \to \eta\Lambda\pi^+$ and $\eta\Sigma^0\pi^+$ decays are calculated relative to that for $\Lambda_c^+ \to pK^-\pi^+$ using the efficiency-corrected event yields via the following equation,

$$\frac{\mathcal{B}(\text{Decay Mode})}{\mathcal{B}(\Lambda_c^+ \to pK^-\pi^+)} = \frac{y(\text{Decay Mode})}{\mathcal{B}_{\text{PDG}} \times y(\Lambda_c^+ \to pK^-\pi^+)}, \quad (1)$$

where decay mode is either $\Lambda_c^+ \to \eta\Lambda\pi^+$ or $\Lambda_c^+ \to \eta\Sigma^0\pi^+$, and $y(\text{Decay Mode})$ refers to the efficiency-corrected yield of the corresponding decay mode. Here $\mathcal{B}_{\text{PDG}}$ denotes subdecay branching fractions of the η, Λ, and Σ^0; we use $\mathcal{B}(\eta \to \gamma\gamma) = (39.41 \pm 0.20)\%$, $\mathcal{B}(\Lambda \to p\pi^-) = (63.9 \pm 0.5)\%$, and $\mathcal{B}(\Sigma^0 \to \Lambda\gamma) = 100\%$ from Ref. [22].

Figure 1 shows the $M(\eta\Lambda\pi^+)$ spectrum after the application of the event selection described in the previous section. In this spectrum, there is a peaking structure at 2.286 GeV/c^2 that corresponds to the $\Lambda_c^+ \to \eta\Lambda\pi^+$ channel. The enhancement to the left of the peak corresponds to the $\Lambda_c^+ \to \eta\Sigma^0\pi^+$ channel with a missing photon from the $\Sigma^0 \to \Lambda\gamma$ decay. We perform a binned-χ^2 fit to the $M(\eta\Lambda\pi^+)$ distribution to extract the $\Lambda_c^+ \to \eta\Sigma^0\pi^+$ signal yield. The probability density functions (PDFs) of the signals are modeled empirically based on MC samples as the sum of a Gaussian and two bifurcated Gaussian functions with a common mean for $\Lambda_c^+ \to \eta\Lambda\pi^+$, and a histogram PDF for the feed-down of the $\Lambda_c^+ \to \eta\Sigma^0\pi^+$ decay. The latter PDF is derived from $\Lambda_c^+ \to \eta\Sigma^0\pi^+$; $\Sigma^0 \to \Lambda\gamma$ decays where the photon decaying from the Σ^0 is not reconstructed. The PDF of the combinatorial backgrounds used for the fit is a third-order polynomial function. The signal yield for the feed-down from the $\Lambda_c^+ \to \eta\Sigma^0\pi^+$ channel shown in Fig. 1 is 17058 ± 871. This yield is then corrected for the reconstruction efficiency obtained from MC to give an efficiency-corrected yield of $(3.05 \pm 0.16) \times 10^5$, where the uncertainty is statistical only.

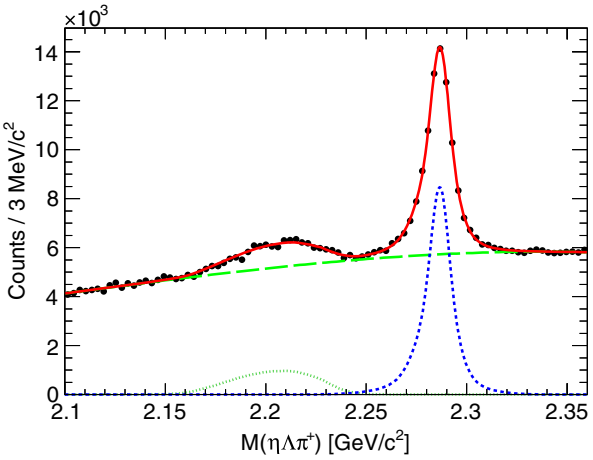

FIG. 1. Fit to the $M(\eta\Lambda\pi^+)$ distribution. The curves indicate the fit result: the total PDF (solid red), signal from $\Lambda_c^+ \to \eta\Sigma^0\pi^+$ channel with a missing photon from the Σ^0 decay (dotted dark green), signal from $\Lambda_c^+ \to \eta\Lambda\pi^+$ decay (dashed blue) and combinatorial backgrounds (long-dashed green).

The $\Lambda_c^+ \to \eta\Lambda\pi^+$ and $pK^-\pi^+$ channels have sufficiently large statistics to allow for yield extractions in individual bins of the Dalitz plot, in order to take into account the bin-to-bin variations of the efficiencies. Figure 2 shows the Dalitz plot bins and their efficiencies for $\Lambda_c^+ \to \eta\Lambda\pi^+$ and $pK^-\pi^+$, respectively. For the fit to each bin of the $\Lambda_c^+ \to \eta\Lambda\pi^+$ Dalitz plot, we use PDFs of the same form described above. In the $pK^-\pi^+$ channel, two Gaussian functions sharing a common mean value and a third-order polynomial function are used to represent the $pK^-\pi^+$ signals and combinatorial backgrounds, respectively. For the signal PDFs in both the $\Lambda_c^+ \to \eta\Lambda\pi^+$ and $pK^-\pi^+$ fits, all parameters except for normalizations are fixed for each bin. The fixed parameters are first obtained for each bin according to an MC simulation and later corrected by taking into account the difference of the fit results between data and MC samples over the entire region of the Dalitz plot. For the fit to $\Lambda_c^+ \to \eta\Lambda\pi^+$, all the parameters for the PDF attributed to the feed-down from the $\Lambda_c^+ \to \eta\Sigma^0\pi^+$ decay with one photon missing are fixed, including the normalization based on the measured yield in this analysis. The polynomial functions for the combinatorial backgrounds are floated for both $\Lambda_c^+ \to \eta\Lambda\pi^+$ and $pK^-\pi^+$ decays. Figures 3 and 4 show examples of fits for three of the Dalitz plot bins. For the $\Lambda_c^+ \to \eta\Lambda\pi^+$ and $pK^-\pi^+$ channels, the extracted yields are efficiency-corrected for

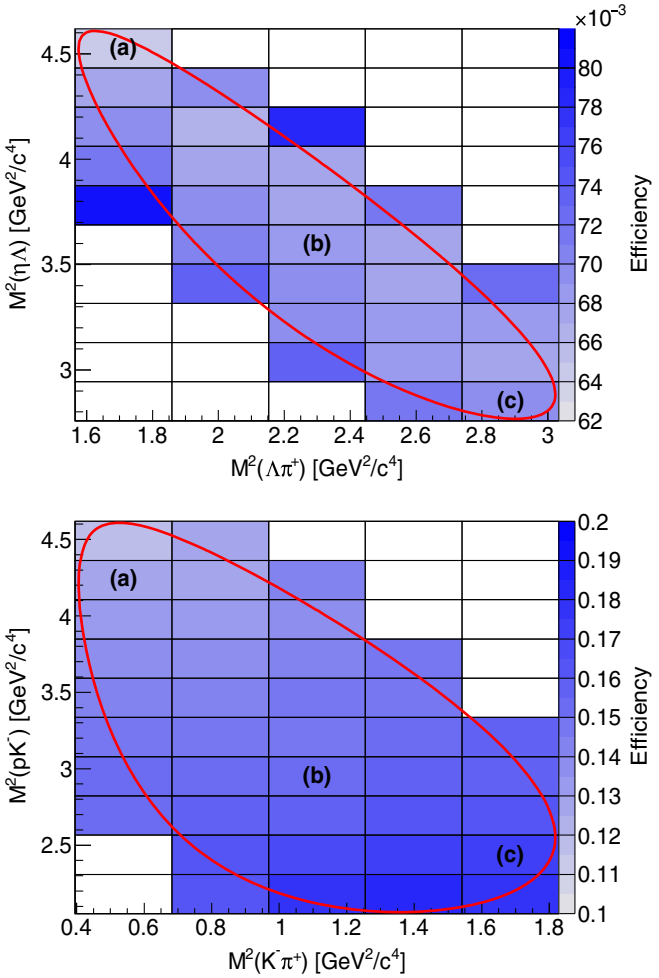

FIG. 2. Distribution of the reconstruction efficiencies over the Dalitz plots divided into the 10×5 bins of $M^2(\Lambda\pi^+)$ vs $M^2(\eta\Lambda)$ for the $\Lambda_c^+ \to \eta\Lambda\pi^+$ channel (top) and of $M^2(K^-\pi^+)$ vs $M^2(pK^-)$ for the $\Lambda_c^+ \to pK^-\pi^+$ channel (bottom). The red lines indicate the Dalitz plot boundaries. The fits in the three sample bins of (a), (b) and (c) are shown in Fig. 3. for the $\Lambda_c^+ \to \eta\Lambda\pi^+$ channel and in Fig. 4 for the $\Lambda_c^+ \to pK^-\pi^+$ channel.

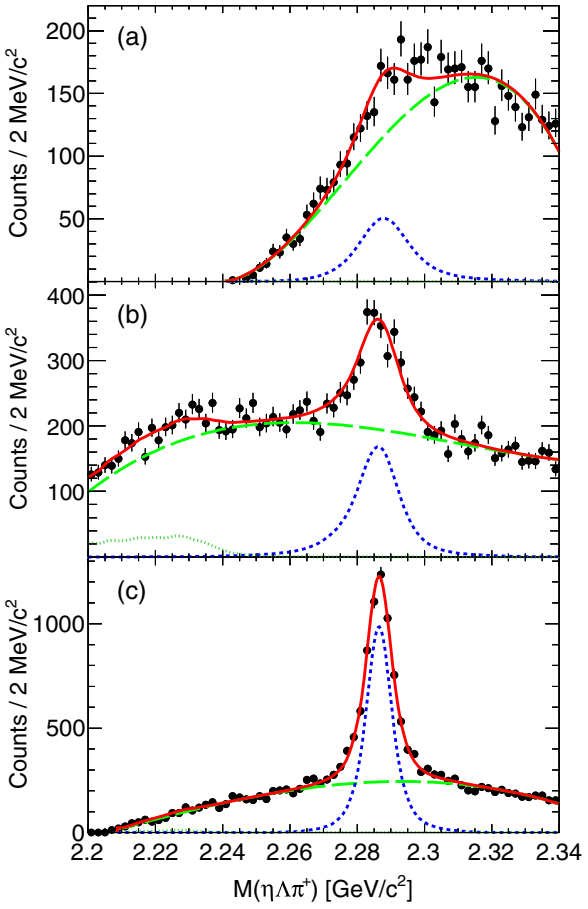

FIG. 3. Fits in three sample Dalitz plot bins (see Fig. 2) of the $\Lambda_c^+ \to \eta\Lambda\pi^+$ channel. The curves indicate the fit results: the total PDF (solid red), signal from the $\Lambda_c^+ \to \eta\Sigma^0\pi^+$ channel with a missing photon from the Σ^0 decay (dotted dark green), signal from the $\Lambda_c^+ \to \eta\Lambda\pi^+$ decay (dashed blue) and combinatorial backgrounds (long-dashed green).

each bin and summed up over the Dalitz plots. The results for the total efficiency-corrected signal yields are summarized in Table I.

We determine the branching fractions using the efficiency-corrected signal yields and Eq. (1). The branching fractions are summarized in Table II.

V. ANALYSIS FOR INTERMEDIATE $\Lambda_c^+ \to \Lambda(1670)\pi^+$ AND $\eta\Sigma(1385)^+$ MODES

Bands corresponding to $\Lambda_c^+ \to \Lambda(1670)\pi^+$ and $\eta\Sigma(1385)^+$ resonant subchannels are evident in the Dalitz plot of $M^2(\Lambda\pi^+)$ versus $M^2(\eta\Lambda)$ shown in Fig. 5. We determine the branching fractions for $\Lambda_c^+ \to \Lambda(1670)\pi^+$ and $\Lambda_c^+ \to \eta\Sigma(1385)^+$ decays using Eq. (1). In this case, "Decay Mode" refers to $\Lambda_c^+ \to \Lambda(1670)\pi^+ \to \eta\Lambda\pi^+$ or $\Lambda_c^+ \to \eta\Sigma(1385)^+$. For the $\Lambda_c^+ \to \eta\Sigma(1385)^+$ decay, $\mathcal{B}_{\rm PDG}$ includes the subdecay branching fraction of $\Sigma(1385)^+ \to \Lambda\pi^+$, $\mathcal{B}(\Sigma(1385)^+ \to \Lambda\pi^+) = 87.0 \pm 1.5\%$ [22]. However, in the case of the $\Lambda_c^+ \to \Lambda(1670)\pi^+$, the subdecay branching fraction of $\Lambda(1670) \to \eta\Lambda$ is not included because of its large uncertainty [22].

In order to extract yields for the $\Lambda_c^+ \to \Lambda(1670)\pi^+$ and $\Lambda_c^+ \to \eta\Sigma(1385)^+$ contributions to inclusive $\Lambda_c^+ \to \eta\Lambda\pi^+$ decays, we fit the $M(\eta\Lambda\pi^+)$ mass distributions, and extract Λ_c^+ signal yields for each 2 MeV/c^2 bin of the $M(\eta\Lambda)$ and $M(\Lambda\pi^+)$ distributions. The same form of PDF described in Sec. IV is used to fit the $M(\eta\Lambda\pi^+)$ mass spectrum, and the PDF parameters for each mass bin are obtained in the same way for the fit of each Dalitz plot bin in Sec. IV. The Λ_c^+ yields as a function of $M(\eta\Lambda)$ and $M(\Lambda\pi^+)$ are shown in Fig. 6. The $\Lambda(1670)$ and $\Sigma(1385)^+$ resonances are clearly evident in Fig. 6(top) and (bottom), respectively. This is the first observation of the $\Lambda(1670)$ in $\Lambda_c^+ \to \eta\Lambda\pi^+$ decays.

To extract the signal yields for the two resonant decay modes, binned least-χ^2 fits are performed to the $M(\eta\Lambda)$ and

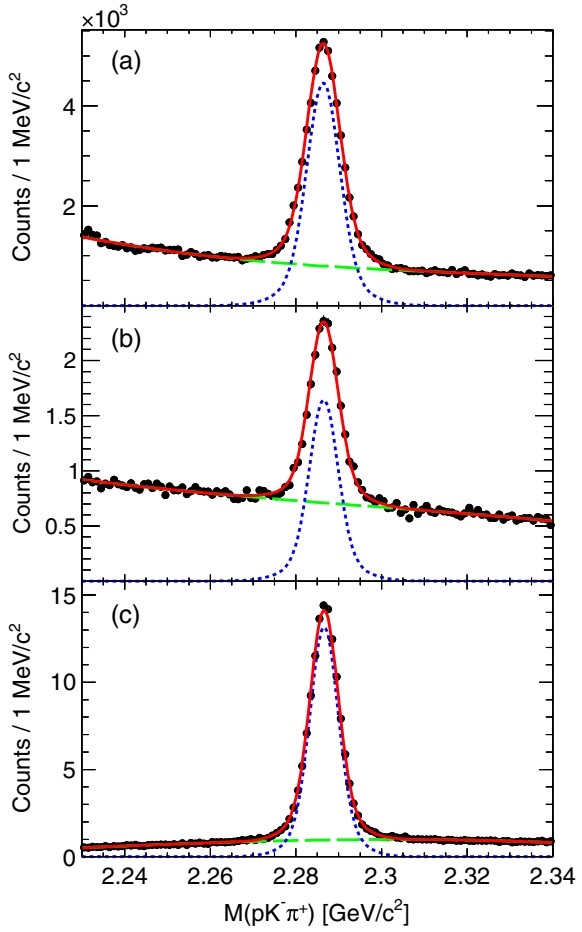

FIG. 4. Fits in three sample Dalitz plot bins (see Fig. 2) of the $\Lambda_c^+ \to pK^-\pi^+$ channel. The curves indicate the fit results: the total PDF (solid red), signal from the $\Lambda_c^+ \to pK^-\pi^+$ decays (dashed blue) and combinatorial backgrounds (long-dashed green).

$M(\Lambda\pi^+)$ spectra shown in Fig. 6. For the signal modeling, we use an S-wave relativistic partial width Breit-Wigner (BW) for the $\Lambda(1670)$ and a corresponding P-wave BW for the $\Sigma(1385)^+$:

TABLE I. Summary of the efficiency-corrected signal yields for the various Λ_c^+ decay modes. The uncertainties are statistical. Note that for the $\Lambda_c^+ \to \eta\Lambda\pi^+$ and $\Lambda_c^+ \to pK^-\pi^+$ decays, the signal yields are corrected in each Dalitz plot bin and summed, unlike the other decays.

Decay modes	Extracted yields	Efficiency-corrected yields $[\times 10^3]$
$\Lambda_c^+ \to \eta\Lambda\pi^+$	51276 ± 454	741 ± 7
$\Lambda_c^+ \to pK^-\pi^+$	1544580 ± 1552	10047 ± 10
$\Lambda_c^+ \to \eta\Sigma^0\pi^+$	17058 ± 871	305 ± 16
$\Lambda_c^+ \to \Lambda(1670)\pi^+$	9760 ± 519	140 ± 7
$\Lambda_c^+ \to \eta\Sigma(1385)^+$	29372 ± 875	423 ± 13

TABLE II. Summary of the branching fractions for the various Λ_c^+ decay modes relative to the $\Lambda_c^+ \to pK^-\pi^+$ mode. The quoted uncertainties are statistical and systematic, respectively.

Decay modes	$\mathcal{B}(\text{Decay mode})/\mathcal{B}(\Lambda_c^+ \to pK^-\pi^+)$
$\Lambda_c^+ \to \eta\Lambda\pi^+$	$0.293 \pm 0.003 \pm 0.014$
$\Lambda_c^+ \to \eta\Sigma^0\pi^+$	$0.120 \pm 0.006 \pm 0.010$
$\Lambda_c^+ \to \Lambda(1670)\pi^+$; $\Lambda(1670) \to \eta\Lambda$	$(5.54 \pm 0.29 \pm 0.73) \times 10^{-2}$
$\Lambda_c^+ \to \eta\Sigma(1385)^+$	$0.192 \pm 0.006 \pm 0.016$

$$\frac{dN}{dm} \propto \frac{m\Gamma(m)}{(m^2 - m_0^2)^2 + m_0^2(\Gamma(m) + \Gamma_{\text{others}})^2}, \tag{2}$$

with

$$\Gamma(m) = \Gamma_0 \frac{m_0}{m}\left(\frac{q}{q_0}\right)^{2L+1} F(q), \tag{3}$$

where m, m_0 and L are the invariant mass, the nominal mass and the decay angular momentum, respectively, and q and q_0 are the center-of-mass momenta corresponding to m and m_0, respectively. Here $\Gamma(m)$ is the partial width for $\Lambda(1670) \to \eta\Lambda$ or $\Sigma(1385)^+ \to \Lambda\pi^+$ and $\Gamma_0 = \Gamma(m_0)$ is a floating parameter in the fit. The contribution Γ_{others}, which indicates the sum of the partial widths for the other decay modes, is fixed to 25 MeV for the $\Lambda(1670)$ and 5 MeV for the $\Sigma(1385)^+$ [22]. Unlike the $\Sigma(1385)^+$, the branching

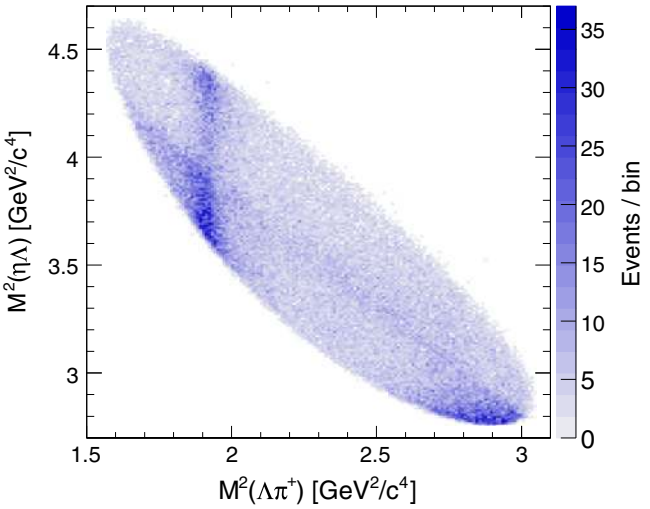

FIG. 5. Dalitz plot, invariant mass squared of $\Lambda\pi^+$ versus $\eta\Lambda$, for the $\Lambda_c^+ \to \eta\Lambda\pi^+$ channel within $2.278\,\text{GeV}/c^2 < M(\eta\Lambda\pi^+) < 2.294\,\text{GeV}/c^2$ in data sample. Both bin widths of the x and y axes are $0.01\text{GeV}^2/c^4$. Over the Dalitz plot, 48% of events are non-Λ_c^+ events. Horizontal and vertical bands at $M^2(\eta\Lambda) = 2.79\ \text{GeV}^2/c^4$ and $M^2(\Lambda\pi^+) = 1.92\ \text{GeV}^2/c^4$ correspond to $\Lambda(1670)\pi^+$ and $\eta\Sigma(1385)^+$ subchannels, respectively. In addition, the diagonal band corresponds to the $a_0(980)^+\Lambda$ subchannel.

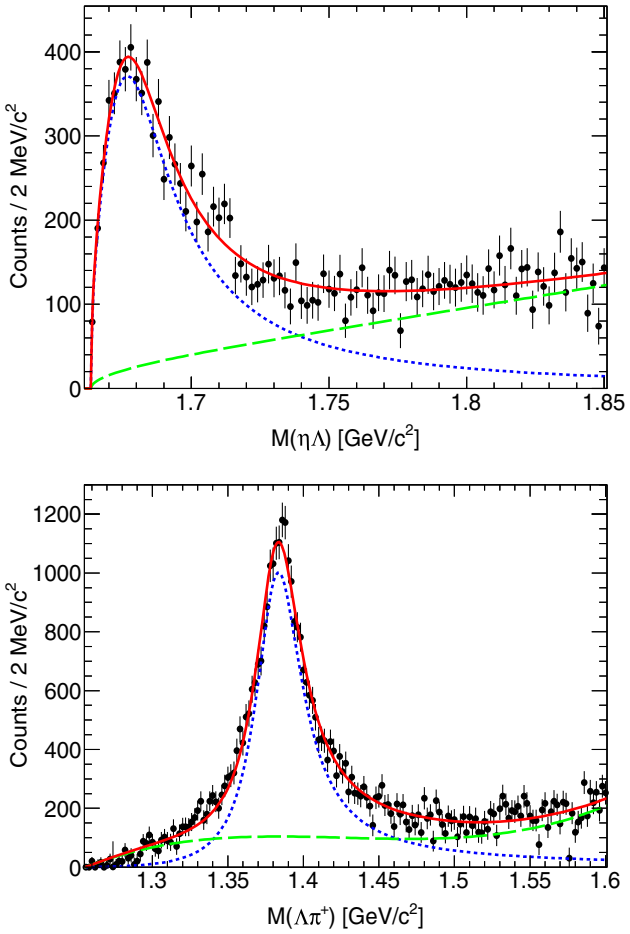

FIG. 6. Fits to the Λ_c^+ yield in the $M(\eta\Lambda)$ (top) and $M(\Lambda\pi^+)$ (bottom) spectra. The curves indicate the fit results: the total PDFs (solid red), the signal PDFs modeled with a relativistic Breit-Wigner function (dashed blue), and the background PDFs (long-dashed green).

fractions for $\Lambda(1670)$ decays are not well determined [22], we select 25 MeV as the nominal value for Γ_{others}. A systematic uncertainty associated with this assignment for Γ_{others} is calculated by changing this value over a wide range from 15 to 32 MeV. In Eq. (3), the Blatt-Weisskopf centrifugal barrier factor $F(q)$ is 1 for S wave and $(1+R^2q_0^2)/(1+R^2q^2)$ for P wave, with $R = 3.1$ GeV^{-1} [23]. The detector resolution for $\Lambda(1670)$ is not included in the signal PDF because the detector response function is not a simple Gaussian near threshold. The effect of this is small and is treated as a systematic uncertainty in the measurement. On the other hand, for the $\Sigma(1385)^+$ the relativistic Breit-Wigner function is convolved with a Gaussian with $\sigma = 1.39$ MeV/c^2 to form the signal PDF. This σ value is determined from a MC simulation of detector responses. To represent the background to the $\Lambda(1670)$ signal, we use a function including a threshold factor: $\sqrt{m-m_{\Lambda\eta}}[p_0+p_1(m-m_{\Lambda\eta})]$, where p_0 and p_1 are free parameters and $m_{\Lambda\eta}$ is the sum of the masses of Λ and η. In the case of the $\Sigma(1385)^+$ fit, a third-order Chebyshev polynomial function is used to represent the background. The χ^2/ndf of the $\Lambda(1670)$ and $\Sigma(1385)^+$ fits are 90.3/90 and 194/167, respectively. We calculate the corresponding reconstruction efficiencies of $\Lambda_c^+ \to \Lambda(1670)\pi^+$ and $\Lambda_c^+ \to \eta\Sigma(1385)^+$ decays from a MC simulation. The extracted yields from the fits in Fig. 6 are divided by the reconstruction efficiencies and the results are summarized in Table I. The branching fractions relative to $\Lambda_c^+ \to pK^-\pi^+$ decay are summarized in Table II.

TABLE III. Results for mass and width of the $\Lambda(1670)$ and $\Sigma(1385)^+$. The first and second uncertainties are statistical and systematic, respectively.

Resonances	Mass [MeV/c^2]	Width [MeV]
$\Lambda(1670)$	$1674.3 \pm 0.8 \pm 4.9$	$36.1 \pm 2.4 \pm 4.8$
$\Sigma(1385)^+$	$1384.8 \pm 0.3 \pm 1.4$	$38.1 \pm 1.5 \pm 2.1$

From the fit results, we also determine masses and widths ($\Gamma_{\text{tot}} = \Gamma_0 + \Gamma_{\text{others}}$) of the $\Lambda(1670)$ and $\Sigma(1385)^+$ as summarized in Table III. Changes in efficiency over the $M(\eta\Lambda)$ and $M(\Lambda\pi^+)$ distributions are not considered because their effect is negligible as described in Sec. VI. The results obtained for the $\Sigma(1385)^+$ are consistent with previous measurements [22]. For the $\Lambda(1670)$, the mass and width have not been previously measured directly from a peaking structure in the mass distribution. The values that we obtain fall within the range of the partial wave analyses of the $\bar{K}N$ reaction [9,10].

VI. SYSTEMATIC UNCERTAINTIES

The systematic uncertainties for the $\Lambda_c^+ \to \eta\Lambda\pi^+$, $\eta\Sigma^0\pi^+$, and $pK^-\pi^+$ efficiency-corrected yields are listed in Table IV. A study is performed based on a $D^{*+} \to D^0\pi^+(D^0 \to K^-\pi^+)$ control sample for πK identification and on the $\Lambda \to p\pi^-$ decay for the proton identification to give corrections for the reconstruction efficiencies and to evaluate the systematic uncertainties due to the PID

TABLE IV. Summary of the systematic uncertainties (in %) in the efficiency-corrected yields for the $\Lambda_c^+ \to \eta\Lambda\pi^+$, $\Lambda_c^+ \to \eta\Sigma^0\pi^+$ and $\Lambda_c^+ \to pK^-\pi^+$ channels.

Source	$\eta\Lambda\pi^+$	$\eta\Sigma^0\pi^+$	$pK^-\pi^+$
PID	1.1	1.1	1.4
Λ reconstruction	2.8	2.8	–
η reconstruction	3.0	3.0	–
Dalitz plot binning	1.3	–	0.7
Intermediate states	–	6.7	–
Background PDF	0.6	0.8	0.4
MC statistics	0.2	0.2	0.1
$\mathcal{B}_{\text{PDG}}$	0.9	0.9	–
Total	4.6	8.0	1.6

selection. Conservatively, all PID systematic uncertainties are considered to be independent when calculating the relative branching fractions to the $\Lambda_c^+ \to pK^-\pi^+$ channel. The systematic uncertainty due to Λ reconstruction is determined from a comparison of yield ratios of $B \to \Lambda\bar{\Lambda}K^+$ with and without the Λ selection cut in data and MC samples. The weighted average of the difference between data and MC samples over the momentum range is assigned as the systematic uncertainty. A 3.0% systematic uncertainty attributed to η reconstruction is assigned by comparing the MC and data ratios of π^0 reconstruction efficiency for $\eta \to 3\pi^0$ and $\eta \to \pi^+\pi^-\pi^0$ decays [24]. The binning over the Dalitz plots is varied from 10×5 to 6×4 and the differences in the results are taken as a systematic uncertainty. Unlike the $\Lambda_c^+ \to \eta\Lambda\pi^+$ and $\Lambda_c^+ \to pK^-\pi^+$ channels that are analyzed in a model-independent way, the efficiency of the $\Lambda_c^+ \to \eta\Sigma^0\pi^+$ decay mode depends on its substructure. To estimate the effect of possible substructures in the $\Lambda_c^+ \to \eta\Sigma^0\pi^+$ decay, the efficiencies of $\Lambda_c^+ \to \eta\Sigma(1385)^+ \to \eta\Sigma^0\pi^+$, $\Lambda_c^+ \to a_0(980)^+\Sigma^0 \to \eta\Sigma^0\pi^+$, $\Lambda_c^+ \to \eta\Sigma(1670)^+ \to \eta\Sigma^0\pi^+$, $\Lambda_c^+ \to \eta\Sigma(1750)^+ \to \eta\Sigma^0\pi^+$, $\Lambda_c^+ \to \Sigma(1750)^0\pi^+ \to \eta\Sigma^0\pi^+$, and $\Lambda_c^+ \to \Sigma(2030)^0\pi^+ \to \eta\Sigma^0\pi^+$ modes are compared to that of the nonresonant decay mode of $\Lambda_c^+ \to \eta\Sigma^0\pi^+$ which is used to detect the yield, and the largest difference of the individual efficiencies to the nonresonant efficiency is used as the associated systematic uncertainty. The systematic uncertainty due to the background PDF modeling is determined by changing the polynomial function from third order to fourth order.

In addition, the systematic uncertainties from the subdecay mode analysis that are not in common with the $\Lambda_c^+ \to \eta\Lambda\pi^+$ decay channel are summarized in Table V and described below. In order to estimate the systematic uncertainty due to Γ_{others}, its value in the $\Lambda(1670)$ ($\Sigma(1385)^+$) fit is varied from 15 to 32 (2 to 8) MeV and the maximum difference is taken as the systematic uncertainty. The ranges of Γ_{others} conservatively cover the branching fractions of $\Lambda(1670)$ and $\Sigma(1385)^+$ decays in Ref. [22] and the q dependence of Γ_{others} is negligible compared to this systematic uncertainty. In the $M(\eta\Lambda)$ spectrum, the mass resolution varies from 0 to 2 MeV/c^2 depending on mass; thus, two fits are performed by setting the mass resolution to 1 MeV/c^2 and 2 MeV/c^2, and the maximum difference is assigned as a systematic uncertainty. For the $M(\Lambda\pi^+)$ spectrum, we increase the detector resolution by 20% and the resultant change is taken as a systematic uncertainty. The systematic uncertainties from the background PDF modeling are estimated by fits with fixed shapes of background PDFs, which are determined by MC simulations including known background sources such as $\Lambda_c^+ \to a_0(980)^+\Lambda$, nonresonant, and $\Lambda_c^+ \to \eta\Sigma(1385)^+$ ($\Lambda_c^+ \to \Lambda(1670)\pi^+$) decays in the $M(\eta\Lambda)$ [$M(\Lambda\pi^+)$] spectrum. In order to consider systematic uncertainties related to angular distributions of $\Lambda(1670)$ and $\Sigma(1385)^+$, the efficiencies in 10 bins of helicity angle are calculated and the largest efficiency differences between any efficiency in the helicity angle bin and the efficiency used to correct the yields are taken as systematic uncertainties. It is possible that the results for the $\Lambda(1670)$ and $\Sigma(1385)^+$ can be affected by another resonant channel, $\Lambda_c^+ \to a_0(980)^+\Lambda$. To account for the interference effect with $a_0(980)^+$, we apply an additional $a_0(980)^+$ veto selection, removing events from 0.95 to 1.02 GeV/c^2 of $M(\eta\pi^+)$, to the $M(\eta\Lambda)$ and $M(\Lambda\pi^+)$ distributions and subsequently repeat the fits. By comparing the fit results with and without the $a_0(980)^+$ requirement, we determine the systematic uncertainties in the masses and widths. For the efficiency-corrected yields, the expected yields calculated on the assumption that there is no interference effect are compared to the nominal values. Since the centrifugal barrier factor [23] is a model-dependent parameter, it has a sizeable uncertainty. Varying the parameter R by ± 0.3 GeV^{-1}, fits are performed to estimate the systematic uncertainty. We also assign a systematic uncertainty from binning of $M(\eta\Lambda)$ and $M(\Lambda\pi^+)$ distributions that is determined by changing the bin widths to 1 MeV/c^2. In the $\Lambda(1670)$ study, we assume that the effects of other neighboring Λ^* hyperons such as $\Lambda(1600)$, $\Lambda(1690)$, and $\Lambda(1710)$ are negligible. These Λ^* hyperons are not observed in the $\Lambda\eta$ mode, and recent measurements on the other modes imply $\Lambda(1600/1690/1710) \to \Lambda\eta$ decays are not significant [9,10,25].

The systematic uncertainties for the mass and width measurements are listed in Table VI. In the same way as described above, the systematic uncertainties from the PDFs and the binning of the $\Lambda(1670)$ and $\Sigma(1385)^+$ fits are estimated. The absolute mass scaling is determined by comparing the measured mass of Λ_c^+ with that in Ref. [22], and it is considered as a systematic uncertainty. To estimate

TABLE V. Summary of the systematic uncertainties (in %) in the efficiency-corrected yields for the $\Lambda_c^+ \to \Lambda(1670)\pi^+$ and $\Lambda_c^+ \to \eta\Sigma(1385)^+$ channels that are not shared with $\Lambda_c^+ \to \eta\Lambda\pi^+$ channel. The last row gives the total systematic uncertainty (and including the common sources, which are Λ reconstruction and η reconstruction listed in Table IV).

Source	$\Lambda(1670)$	$\Sigma(1385)^+$
PID	1.0	1.1
Γ_{others}	2.1	1.4
Detector resolution	1.6	1.8
Background modeling	11.6	2.8
Efficiency variation over helicity angle	1.8	5.5
Centrifugal barrier	–	0.7
$\mathcal{B}_{\text{PDG}}$	0.9	2.0
MC statistics	0.2	0.2
Bin width	1.7	1.2
Interference with $a_0(980)^+$	1.5	0.6
Total	12.4 (13.0)	7.1 (8.2)

TABLE VI. Summary of the systematic uncertainties in the masses and widths for the $\Lambda(1670)$ and $\Sigma(1385)^+$.

	$\Lambda(1670)$		$\Sigma(1385)^+$	
Source	Mass [MeV/c^2]	Width [MeV]	Mass [MeV/c^2]	Width [MeV]
Γ_{others}	3.6	2.0	0.3	0.8
Detector resolution	0.4	0.5	0.0	0.8
Background modeling	0.9	3.9	0.4	1.5
Centrifugal barrier	–	–	0.1	0.6
Bin width	0.0	0.8	0.1	0.7
Mass scaling	0.2	–	0.2	–
Efficiency correction	0.1	0.0	0.1	0.2
Interference with $a_0(980)^+$	3.1	1.5	1.3	0.2
Total	4.9	4.8	1.4	2.1

the systematic uncertainty due to the $M(\eta\Lambda)$- and $M(\Lambda\pi^+)$-dependent reconstruction efficiencies, we apply reconstruction efficiency corrections to the $M(\eta\Lambda)$ and $M(\Lambda\pi^+)$ spectra. For the corrections, we calculate the mass dependencies of these efficiencies by MC simulation. They are found to vary between 0.068 and 0.070 for $M(\eta\Lambda)$ and between 0.069 and 0.071 for $M(\Lambda\pi^+)$, and in both cases the behavior is nearly flat. The mass spectra are divided by these efficiencies. Differences in fit results with and without the efficiency corrections are negligible compared to these other systematic sources as listed in Table VI.

VII. SUMMARY

We analyze the $\eta\Lambda\pi^+$ final state to study Λ_c^+ decays using the full data set of 980 fb^{-1} at or near the $\Upsilon(nS)$ resonances collected by the Belle detector. Two new decay modes of the Λ_c^+ baryon, $\Lambda_c^+ \to \eta\Sigma^0\pi^+$ and $\Lambda_c^+ \to \Lambda(1670)\pi^+$, are observed for the first time, and their branching fractions are measured relative to that of the $\Lambda_c^+ \to pK^-\pi^+$ decay mode. In addition, the branching fractions for $\Lambda_c^+ \to \eta\Lambda\pi^+$ and $\Lambda_c^+ \to \eta\Sigma(1385)^+$, which were reported previously by CLEO [11] and by BESIII [12], are measured with much improved precision. The results are

$$\frac{\mathcal{B}(\Lambda_c^+ \to \eta\Lambda\pi^+)}{\mathcal{B}(\Lambda_c^+ \to pK^-\pi^+)} = 0.293 \pm 0.003 \pm 0.014,$$
$$\frac{\mathcal{B}(\Lambda_c^+ \to \eta\Sigma^0\pi^+)}{\mathcal{B}(\Lambda_c^+ \to pK^-\pi^+)} = 0.120 \pm 0.006 \pm 0.010,$$
$$\frac{\mathcal{B}(\Lambda_c^+ \to \Lambda(1670)\pi^+) \times \mathcal{B}(\Lambda(1670) \to \eta\Lambda)}{\mathcal{B}(\Lambda_c^+ \to pK^-\pi^+)} = (5.54 \pm 0.29 \pm 0.73) \times 10^{-2},$$

and

$$\frac{\mathcal{B}(\Lambda_c^+ \to \eta\Sigma(1385)^+)}{\mathcal{B}(\Lambda_c^+ \to pK^-\pi^+)} = 0.192 \pm 0.006 \pm 0.016,$$

where the uncertainties, here and below, are statistical and systematic, respectively. Using the world average value $\mathcal{B}(\Lambda_c^+ \to pK^-\pi^+) = (6.28 \pm 0.32)\%$ [22], the absolute branching fractions are determined to be

$$\mathcal{B}(\Lambda_c^+ \to \eta\Lambda\pi^+) = (1.84 \pm 0.02 \pm 0.09 \pm 0.09)\%,$$
$$\mathcal{B}(\Lambda_c^+ \to \eta\Sigma^0\pi^+) = (7.56 \pm 0.39 \pm 0.62 \pm 0.39) \times 10^{-3},$$
$$\mathcal{B}(\Lambda_c^+ \to \Lambda(1670)\pi^+) \times \mathcal{B}(\Lambda(1670) \to \eta\Lambda) = (3.48 \pm 0.19 \pm 0.46 \pm 0.18) \times 10^{-3},$$

and

$$\mathcal{B}(\Lambda_c^+ \to \eta\Sigma(1385)^+) = (1.21 \pm 0.04 \pm 0.10 \pm 0.06)\%,$$

where the third uncertainty is from $\mathcal{B}(\Lambda_c^+ \to pK^-\pi^+)$. The branching fractions relative to $\Lambda_c^+ \to \eta\Lambda\pi^+$, excluding $\Lambda_c^+ \to pK^-\pi^+$, are

$$\frac{\mathcal{B}(\Lambda_c^+ \to \eta\Sigma^0\pi^+)}{\mathcal{B}(\Lambda_c^+ \to \eta\Lambda\pi^+)} = 0.411 \pm 0.021 \pm 0.028,$$
$$\frac{\mathcal{B}(\Lambda_c^+ \to \Lambda(1670)\pi^+) \times \mathcal{B}(\Lambda(1670) \to \eta\Lambda)}{\mathcal{B}(\Lambda_c^+ \to \eta\Lambda\pi^+)} = 0.189 \pm 0.010 \pm 0.023,$$

and

$$\frac{\mathcal{B}(\Lambda_c^+ \to \eta\Sigma(1385)^+)}{\mathcal{B}(\Lambda_c^+ \to \eta\Lambda\pi^+)} = 0.656 \pm 0.020 \pm 0.046,$$

where the systematic uncertainties from PID, Λ reconstruction, η reconstruction, $\mathcal{B}(\Lambda \to p\pi^-)$, and $\mathcal{B}(\eta \to \gamma\gamma)$ sources in Tables IV and V cancel. The measurements of $\mathcal{B}(\Lambda_c^+ \to \eta\Lambda\pi^+)$ and $\mathcal{B}(\Lambda_c^+ \to \eta\Sigma(1385)^+)$ are the most precise results to date and agree with earlier results reported by CLEO [11] and by BESIII [12]. In our study, the mass and width of the $\Lambda(1670)$ and $\Sigma(1385)^+$ are also determined to be

$$m_0(\Lambda(1670)) = 1674.3 \pm 0.8 \pm 4.9 \text{ MeV}/c^2,$$
$$\Gamma_{\text{tot}}(\Lambda(1670)) = 36.1 \pm 2.4 \pm 4.8 \text{ MeV},$$
$$m_0(\Sigma(1385)^+) = 1384.8 \pm 0.3 \pm 1.4 \text{ MeV}/c^2,$$

and

$$\Gamma_{\text{tot}}(\Sigma(1385)^+) = 38.1 \pm 1.5 \pm 2.1 \text{ MeV}.$$

These are the first measurements of the $\Lambda(1670)$ mass and width that are determined directly from a peaking structure in the mass distribution.

ACKNOWLEDGMENTS

We thank the KEKB group for the excellent operation of the accelerator; the KEK cryogenics group for the efficient operation of the solenoid; and the KEK computer group, and the Pacific Northwest National Laboratory (PNNL) Environmental Molecular Sciences Laboratory (EMSL) computing group for strong computing support; and the National Institute of Informatics, and Science Information NETwork 5 (SINET5) for valuable network support. We acknowledge support from the Ministry of Education, Culture, Sports, Science, and Technology (MEXT) of Japan, the Japan Society for the Promotion of Science (JSPS), and the Tau-Lepton Physics Research Center of Nagoya University; the Australian Research Council including Grants No. DP180102629, No. DP170102389, No. DP170102204, No. DP150103061, No. FT130100303; Austrian Science Fund (FWF); the National Natural Science Foundation of China under Contracts No. 11435013, No. 11475187, No. 11521505, No. 11575017, No. 11675166, No. 11705209; Key Research Program of Frontier Sciences, Chinese Academy of Sciences (CAS), Grant No. QYZDJ-SSW-SLH011; the CAS Center for Excellence in Particle Physics (CCEPP); the Shanghai Pujiang Program under Grant No. 18PJ1401000; the Ministry of Education, Youth and Sports of the Czech Republic under Contract No. LTT17020; the Carl Zeiss Foundation, the Deutsche Forschungsgemeinschaft, the Excellence Cluster Universe, and the VolkswagenStiftung; the Department of Science and Technology of India; the Istituto Nazionale di Fisica Nucleare of Italy; National Research Foundation (NRF) of Korea Grants No. 2016R1D1A1B01010135, No. 2016-R1D1A1B02012900, No. 2018R1A2B3003643, No. 2018R1A6A1A06024970, No. 2018R1D1A1-B07047294, No. 2019K1A3A7A09033840, No. 2019-R1I1A3A01058933; Radiation Science Research Institute, Foreign Large-size Research Facility Application Supporting project, the Global Science Experimental Data Hub Center of the Korea Institute of Science and Technology Information and KREONET/GLORIAD; the Polish Ministry of Science and Higher Education and the National Science Center; the Ministry of Science and Higher Education of the Russian Federation, Agreement 14.W03.31.0026; University of Tabuk research Grants No. S-1440-0321, No. S-0256-1438, and No. S-0280-1439 (Saudi Arabia); the Slovenian Research Agency; Ikerbasque, Basque Foundation for Science, Spain; the Swiss National Science Foundation; the Ministry of Education and the Ministry of Science and Technology of Taiwan; and the United States Department of Energy and the National Science Foundation. J. Y. Lee and S. K. Kim were supported by NRF Grant No. 2016R1A2B3008343. S. B. Yang and J. K. Ahn acknowledges support from NRF Grants No. 2018R1A6A3A01012138 and No 2018R1A5A1025563. Y. Kato is supported by MEXT KAKENHI Grant No. JP19H05148.

[1] T. Uppal, R. C. Verma, and M. P. Khann, Phys. Rev. D **49**, 3417 (1994).
[2] J. G. Körner, M. Krämer, and J. Willrodt, Z. Phys. C **2**, 117 (1979).
[3] A. Zupanc *et al.* (Belle Collaboration), Phys. Rev. Lett. **113**, 042002 (2014).
[4] M. Ablikim *et al.* (BESIII Collaboration), Phys. Rev. Lett. **116**, 052001 (2016).
[5] Unless otherwise stated, charge-conjugate modes are always implied throughout this paper.
[6] J. J. Xie and L. S. Geng, Eur. Phys. J. C **76**, 496 (2016).
[7] R. Koniuk and N. Isgur, Phys. Rev. D **21**, 1868 (1980).
[8] E. Oset, A. Ramos, and C. Bennhold, Phys. Lett. B **527**, 99 (2002).
[9] H. Zhang, J. Tulpan, M. Shrestha, and D. M. Manley, Phys. Rev. C **88**, 035205 (2013).
[10] H. Kamano, S. X. Nakamura, T.-S. H. Lee, and T. Sato, Phys. Rev. C **92**, 025205 (2015).
[11] R. Ammar *et al.* (CLEO Collaboration), Phys. Rev. Lett. **74**, 3534 (1995).
[12] M. Ablikim *et al.* (BESIII Collaboration), Phys. Rev. D **99**, 032010 (2019).
[13] S. Kurokawa and E. Kikutani, Nucl. Instrum. Methods Phys. Res., Sect. A **499**, 1 (2003), and other papers included in this volume; T. Abe *et al.*, Prog. Theor. Exp. Phys. (**2013**), 03A001, and references therein.
[14] A. Abashian *et al.* (Belle Collaboration), Nucl. Instrum. Methods Phys. Res., Sect. A **479**, 117 (2002); also see detector section in J. Brodzicka *et al.*, Prog. Theor. Exp. Phys. (**2012**), 04D001.
[15] T. Sjöstrand, S. Mrenna, and P. Skands, J. High Energy Phys. 05 (2006) 026.
[16] D. Lange, Nucl. Instrum. Methods Phys. Res., Sect. A **462**, 152 (2001); T. Sjöstrand, P. Edén, C. Friberg, L. Lönnblad, G. Miu, S. Mrenna, and E. Norrbin, Comput. Phys. Commun. **135**, 238 (2001).
[17] R. Brun *et al.*, CERN Report No. DD/EE/84-1, 1984.

[18] E. Barberio and Z. Was, Comput. Phys. Commun. **79**, 291 (1994).
[19] S. B. Yang *et al.* (Belle Collaboration), Phys. Rev. Lett. **117**, 011801 (2016).
[20] E. Won *et al.* (Belle Collaboration), Phys. Rev. Lett. **107**, 221801 (2011).
[21] K. Hanagaki, H. Kakuno, H. Ikeda, T. Iijima, and T. Tsukamoto, Nucl. Instrum. Methods Phys. Res., Sect. A **485**, 490 (2002).
[22] P. A. Zyla *et al.* (Particle Data Group), Prog. Theor. Exp. Phys. (**2020**), 083C01.
[23] F. V. Hippel and C. Quigg, Phys. Rev. D **5**, 624 (1972).
[24] M. C. Chang *et al.* (Belle Collaboration), Phys. Rev. D **85**, 091102(R) (2012).
[25] A. V. Sarantsev, M. Matveev, V. A. Nikonov, A. V. Anisovich, U. Thoma, and E. Klempt, Eur. Phys. J. A **55**, 180 (2019).